Ripoll, J. F., Loridan, V., Cunningham, G. S., Reeves, G. D., Shprits, Y. (2016): On the Time Needed to Reach an Equilibrium Structure of the Radiation Belts. - *Journal of Geophysical Research*, *121*, 8, pp. 7684—7698.

DOI: http://doi.org/10.1002/2015JA022207

AGU PUBLICATIONS

JGR

Journal of Geophysical Research: Space Physics

RESEARCH ARTICLE
10.1002/2015JA022207

Key Points:
- The time to reach equilibrium value has a complex scissor shape in (L, *E*)
- Equilibrium value only reachable for selected and determined (L, *E*, *Kp*)
- Dynamics and equilibrium S shape of the belts as in VAP observations

Supporting Information:
- Supporting Information S1

Correspondence to:
J.-F. Ripoll,
jean-francois.ripoll@cea.fr

Citation:
Ripoll, J.-F., V. Loridan, G. S. Cunningham, G. D. Reeves, and Y. Y. Shprits (2016), On the time needed to reach an equilibrium structure of the radiation belts, *J. Geophys. Res. Space Physics*, *121*. 7684–7698, doi:10.1002/2015JA022207.

Received 25 NOV 2015
Accepted 2 JUN 2016
Accepted article online 4 JUN 2016
Published online 22 AUG 2016

On the time needed to reach an equilibrium structure of the radiation belts

J.-F. Ripoll[1], V. Loridan[1], G. S. Cunningham[2], G. D. Reeves[2], and Y. Y. Shprits[3,4]

[1]DAM, DIF, CEA, Arpajon, France, [2]Los Alamos National Laboratory, Los Alamos, New Mexico, USA, [3]Helmholtz Center Potsdam, GFZ, German Research Centre For Geosciences, Germany and University of Potsdam, Potsdam, Germany, [4]Department of Earth, Planetary, and Space Sciences, University of California, Los Angeles, California, USA

Abstract In this study, we complement the notion of equilibrium states of the radiation belts with a discussion on the dynamics and time needed to reach equilibrium. We solve for the equilibrium states obtained using 1-D radial diffusion with recently developed hiss and chorus lifetimes at constant values of $Kp = 1$, 3, and 6. We find that the equilibrium states at moderately low *Kp*, when plotted versus L shell (L) and energy (*E*), display the same interesting S shape for the inner edge of the outer belt as recently observed by the Van Allen Probes. The S shape is also produced as the radiation belts dynamically evolve toward the equilibrium state when initialized to simulate the buildup after a massive dropout or to simulate loss due to outward diffusion from a saturated state. Physically, this shape, intimately linked with the slot structure, is due to the dependence of electron loss rate (originating from wave-particle interactions) on both energy and L shell. Equilibrium electron flux profiles are governed by the Biot number ($\tau_{Diffusion}/\tau_{loss}$), with large Biot number corresponding to low fluxes and low Biot number to large fluxes. The time it takes for the flux at a specific (L, *E*) to reach the value associated with the equilibrium state, starting from these different initial states, is governed by the initial state of the belts, the property of the dynamics (diffusion coefficients), and the size of the domain of computation. Its structure shows a rather complex *scissor* form in the (L, *E*) plane. The equilibrium value (phase space density or flux) is practically reachable only for selected regions in (L, *E*) and geomagnetic activity. Convergence to equilibrium requires hundreds of days in the inner belt for $E > 300$ keV and moderate Kp ($\lesssim 3$). It takes less time to reach equilibrium during disturbed geomagnetic conditions ($Kp \geq 3$), when the system evolves faster. Restricting our interest to the slot region, below $L = 4$, we find that only small regions in (L, *E*) space can reach the equilibrium value: $E \sim [200, 300]$ keV for $L = [3.7, 4]$ at $Kp = 1$, $E \sim [0.6, 1]$ MeV for $L = [3, 4]$ at $Kp = 3$, and $E \sim 300$ keV for $L = [3.5, 4]$ at $Kp = 6$ assuming no new incoming electrons.

1. Introduction

Over 40 years ago, *Lyons and Thorne* [1973] published a study on the equilibrium structure of the radiation belts, which has become a cornerstone of radiation belt physics over the years. The calculations showed a region devoid of electrons, the slot region, created by scattering from hiss waves and located in between two radiation belts, the inner and the outer belt. By assumption, the solution is obtained by balancing electron loss and electron transport. This paper has been highly influential, but our understanding has evolved with successive satellite missions, as the CRRES mission observations showed the dynamics of fluxes down to the slot region [e.g., *Meredith et al.*, 2006; *Shprits et al.*, 2005; *Kim et al.*, 2011; *Friedel et al.*, 1996; *Korth et al.*, 2000], the SAMPEX mission showed the dynamics of fluxes in the slot region [e.g., *Baker et al.*, 2007; *Meredith et al.*, 2006, 2009; *Selesnick*, 2015], the HEO mission showed a quiet inner belt and a "third" belt [e.g., *Fennell et al.*, 2012; *Ripoll et al.*, 2014a, 2014b] (referred to a few years later as "remnant belts" when observed from the Van Allen Probes [*Shprits et al.*, 2013; *Turner et al.*, 2013; *Baker et al.*, 2013]). With the Van Allen Probes mission, one of the important discoveries is a low-energy inner belt [*Fennell et al.*, 2015], with the flux of electrons dropping steeply above 800 keV, possibly explained by a physical *barrier* [*Baker et al.*, 2014] made of vanishing radial transport and/or hiss scattering, in both an equilibrium state (or not). But do these findings reconcile with the equilibrium state of the belts pictured four decades ago? How do we explain a low-energy inner belt while the equilibrium state shows significant fluxes at higher energy? Is the *barrier* an equilibrium state? This study intends to advance our understanding to answer these questions. In particular, it addresses the rather basic question of how long it takes to reach an equilibrium state of the belts, in order to see if that equilibrium state is meaningful. Another motivation relates to the relatively small amount of computation time it requires to calculate

the equilibrium solution (tens of seconds or minutes; cf. equation (3), below), which would allow a very fast estimation of the belts structure, if the equilibrium state was proven to be relevant. Therefore, there is an interest in characterizing when the phase space density values of the equilibrium state at a given (L, *E*) are relevant or not, because, if they were relevant, one could roughly and quickly estimate the radiation dose on satellites. On the other hand, one would strongly overestimate the dose in the inner belt (or underestimate it in the slot) if the time to reach the equilibrium values was too long to be realistic compared to changes of the magnetospheric conditions. Since the dynamics are highly energy-dependent, our study is conducted for all energies and L shells. A wide range of solutions is given in order to compare with current observations, with one solution reproducing the recently observed "S shape" [*Reeves et al*., 2016] of the inner edge of the outer belt when represented in two dimensions as a function of energy and L shell. The formulation we use here, a combination of 1-D radial diffusion and loss terms, is also commonly used in the literature for simulating the radiation belt dynamics during particular events, as, for instance, the October 1990 storm [*Brautigam and Albert*, 2000; *Albert et al*., 2009] or the full year 1990 [*Ozeke et al*., 2014], storms observed in 2002 from GPS satellites [*Tu et al*., 2009], and the month of March 2013 observed from the Van Allen Probes [*Li et al*., 2014]. However, in the present work, no dynamic boundary conditions are used, which assumes that the magnetospheric conditions must be steady during the time of interest. We use recently developed models for electron lifetime due to pitch angle scattering from hiss and chorus, which depend on energy and L shell [*Orlova et al*., 2014; *Orlova and Shprits*, 2014]. To the best of our knowledge, the only past study that compared steady state and time-dependent solutions was done with a primitive electron lifetime model (constant values) [*Shprits and Thorne*, 2004], not energy-dependent models computed from full diffusion coefficients. In section 2, we describe the models that are used in this study. In section 3, we compute equilibrium solutions for different values of *Kp*. In section 4, we compute the time-dependent solution and the time required to reach the equilibrium value as a function of (L, *E*) for two classes of problem: an injection of electrons into a magnetosphere void of electrons after a massive dropout and the decay of a saturated magnetosphere after massive injections.

2. Models

The time evolution of the gyro, bounce, and drift phase-averaged distribution function, *f*(*t*, L, μ, *K*), in the presence of pitch angle diffusion and radial diffusion can be described by the following equation [*Schulz and Lanzerotti*, 1974; *Shprits et al*., 2008]:

$$\frac{\partial f}{\partial t} = L^2 \frac{\partial}{\partial L}\bigg|_{\mu,K}\left(\frac{D_{LL}}{L^2}\frac{\partial f}{\partial L}\bigg|_{\mu,K}\right) + \frac{1}{T(\alpha_0)\sin(2\alpha_0)}\frac{2}{\partial \alpha_0}\bigg|_{L,E}\left(\sum_i D^i_{\alpha_0\alpha_0} T(\alpha_0)\sin(2\alpha_0)\frac{\partial f}{\partial \alpha_0}\bigg|_{L,E}\right) \quad (1)$$

This equation is defined within the coordinates (μ, *K*, L), with μ the first adiabatic invariant, *K* proportional to the second adiabatic invariant, *J* ($K = J\sqrt{B_m}/2p$) with B_m the mirror point magnetic field intensity and *p* the electron momentum, and the Roederer L value defined from the third invariant Φ (with $L = 2\pi B_E R_E^2/\Phi$ with B_E the value of the magnetic field at the equatorial point on the Earth surface and R_E the Earth radius). In equation (1), α_0 is the equatorial pitch angle, D_{LL} is the radial diffusion coefficient, $D^i\alpha\alpha$ the *i*th pitch angle diffusion coefficient associated to the *i*th diffusion process, and $T(\alpha_0)$ is proportional to the bounce period. Equation (1) assumes a dipole field and neglects all cross derivatives.

Note that if the radial diffusion coefficient depends on pitch angle, then another diffusion equation has been derived using the fact that simultaneous diffusion in L shell and pitch angle does not conserve μ as well as $\xi = \mu/y^2$ with $y = \sin^2(\alpha_0)$ [*Walt*, 1970; *Schulz and Lanzerotti*, 1974, equation (3.52a); *Roederer*, 1970]. The transformation from μ to ξ yields diffusion equation (cf. equation (3.52a) in *Schulz and Lanzerotti* [1974]) that is a similar to equation (1) but has a different Jacobian, invariants, and power $L^{5/2}$ (instead of L^2). However, because equation (1) is widely used by the community and the difference between using equation (1) and equation (3.52a) in *Schulz and Lanzerotti* [1974] is expected to be minor, we use equation (1) here. If the summed pitch angle diffusion processes $D_{\alpha_0\alpha_0} = \sum_i D^i_{\alpha_0\alpha_0}$ are fast relative to the radial diffusion processes, then we can assume that an "equilibrium" pitch angle distribution exists having the form $f^{(1)}(\alpha_0, t) = e^{-t/\tau} g(\alpha_0)$, where the equilibrium distribution function shape, $g(\alpha_0)$, and electron

lifetime, τ, can be found by solving an inverse integral problem that results from plugging the expression of $f^{(1)}(\alpha_0, t)$ into [*Lyons et al.*, 1972]

$$\frac{\partial f}{\partial t} = \frac{1}{T(\alpha_0)\sin(2\alpha_0)} \frac{\partial}{\partial \alpha_0}\bigg|_{L,E} \left(D_{\alpha_0\alpha_0} T(\alpha_0)\sin(2\alpha_0) \frac{\partial f}{\partial \alpha_0}\bigg|_{L,E} \right) \tag{2}$$

By equilibrium here we mean with respect to the pitch angle diffusion processes. The solution is

$$\tau_i = \frac{\int_{\partial_L}^{\frac{\pi}{2}} g_i(\alpha_0) T(\alpha_0)\sin(2\alpha_0) d\alpha_0}{D^i_{\alpha_0\alpha_0}(\alpha_L) T(\alpha_L)\sin(2\alpha_L) \frac{\partial g_i(\alpha_L)}{\partial \alpha_0}} \tag{3}$$

and

$$g_i(\alpha) = \int_{\alpha_L}^{\alpha} \frac{D^i_{\alpha_0\alpha_0}(\alpha_L) T(\alpha_L)\sin(2\alpha_L) \frac{\partial g_i(\alpha_L)}{\partial \alpha_0}}{D^i_{\alpha_0\alpha_0}(\alpha') T(\alpha')\sin(2\alpha')} \left(1 - \frac{\int_{\alpha_L}^{\alpha'} T(\alpha_0)\sin(2\alpha_0) g_i(\alpha_0) d\alpha_0}{\int_{\partial_L}^{\frac{\pi}{2}} T(\alpha_0)\sin(2\alpha_0) g_i(\alpha_0) d\alpha_0} \right) d\alpha' \tag{4}$$

with α_L the pitch angle at the loss cone. Equations (3) and (4) are coupled recursive integrodifferential equations, which have to be solved numerically. Restricting our attention to the form $f^{(1)}(\alpha_0, t)$ permits us to reduce equation (2) to $\frac{\partial f}{\partial t} = \frac{-f}{\tau}$ and therefore to reduce equation (1) to one single dimension

$$\frac{\partial f}{\partial t} = L^2 \frac{\partial}{\partial L}\bigg|_{\mu,K} \left(\frac{D_{LL}}{L^2} \frac{\partial f}{\partial L}\bigg|_{\mu,K} \right) - \frac{f}{\tau}\bigg|_{L,E} \tag{5}$$

which is the form used by *Lyons and Thorne* [1973]. If there is more than one pitch angle diffusion process, then equations 2–4 can be applied to each process in turn to calculate a lifetime associated with each process, τ_i, and corresponding equilibrium pitch angle distributions. If the pitch angle diffusion processes dominate in different regimes, i.e., at different energies and L shells, then the lifetimes may legitimately be combined as $\frac{1}{\tau} = \sum_i \frac{1}{\tau_i}$ since there is an equation (2) for each process that reduces to $\frac{\partial f}{\partial t} = \frac{-f}{\tau}$. It produces a single effective lifetime to use in equation (5). Of course, the underlying equilibrium pitch angle distribution that holds will depend on which process is dominant. Equation (5) is referred as simplified radial diffusion with a loss term [*Schulz and Lanzerotti*, 1974, p 108; *Walt*, 1970]. The use of equation (5) is correct only when M and J (or K) are conserved or when the pitch angle distribution at all L is in the lowest diffusive mode of the pitch angle diffusion operator and D_{LL} operator is diagonal [*Walt*, 1970]. Moreover, equation (3.50) in *Schulz and Lanzerotti* [1974] in which a different Jacobian, invariants (ξ instead of μ), and power $L^{5/2}$ (instead of L^2) reduces after appropriate changes of variables (cf. equation (4.56) in *Roederer and Zhang* [2014]) to equation (5) [*Walt*, 1970].

Simplifying equation (1) by equation (5) had supposed two intrinsic approximations. First, the form of $f^{(1)}$ implies that the distribution function decays at the same rate for all pitch angles (i.e., there is one dominating decaying mode corresponding to the smallest eigenvalue of the pitch angle diffusion operator). This has been observed at L = 5 [*O'Brien et al.*, 2014] but there exist, mathematically, times for which it is not true for all (L, E) because the time to reach the equilibrium pitch angle distribution is not small compared with the time scale for radial diffusion, as we assume here. We reiterate that the electron lifetime τ_i is the inverse of the lowest eigenvalue of the ith diffusion operator. All other eigenvalues (i.e., modes), which serve for describing the evolution of pitch angle diffusion, are lost in the process of solving equation (2) via equations (3) and (4). Conserving all the eigenvalues of the pitch angle operator is out of the scope of this article but is possible as explained in *Walt* [1970] (cf. also equation (3.52) and following discussion in *Schulz and Lanzerotti* [1974]).

Our calculation of a single lifetime from the lifetimes of the various processes is also an approximation that originates from the second assumption that the various processes are not simultaneously active on the same pitch angle population for a given L shell and energy. If more than one process affects the pitch angle distribution at a given L shell and energy, a more accurate treatment would sum the diffusion coefficients and then apply equations 2–4 to extract a global lifetime. However, in the case of hiss and chorus waves as treated below, the approximation we use is valid because each wave acts on a disjoint spatial domain (hiss within the plasmasphere and chorus waves outside) and Coulomb collisions dominate for very small L (<1.25). Nevertheless, equation (5), which relies on a single lifetime that is the inverse of the sum of inverse lifetimes

from each process, does not properly account for processes that act simultaneously and cannot be expected to have the accuracy of the full formulation (equation (1) or similar), which treats all processes, time scales, and pitch angle populations simultaneously.

Here we will only discuss the dynamics associated with equation (5) in reaching the equilibrium distribution function as a function of L. Thus, we assume that the equilibrium state, i.e., the equilibrium distribution function as a function of L, f^*, such that it satisfies $\frac{\partial f^*}{\partial t} = 0$, and hence $\frac{\partial}{\partial L}\big|_{\mu,K}\left(\frac{D_{LL}}{L^2}\frac{\partial f^*}{\partial L}\big|_{\mu,K}\right) = \frac{f^*}{\tau}\big|_{L,E}$, not treating the question of the time to reach pitch angle diffusion equilibrium. In what follows, we will often call the distribution functions, $f(t, L, \mu, K)$ or $f^*(L, \mu, K)$, with the PSD abbreviation, while, strictly speaking, the phase-space density (PSD) refers to the one distribution function defined in the traditional six-dimensional phase space [*Roederer and Zhang*, 2014]. We consider three pitch angle diffusion processes ($i = 3$), one from Coulomb collisions and two from wave particle interactions from both hiss and chorus waves. The Coulomb collision lifetime is taken from *Lyons and Thorne* [1973] and assumes Coulomb pitch angle scattering and, to a lesser extent, some energy loss. The hiss lifetime models are of two kinds: the historical *Lyons et al.* [1972] model that is used in *Lyons and Thorne* [1973] and the new full and *Kp*-dependent fit models derived from numerical simulations [*Orlova et al.*, 2014] using the Full Diffusion Code [*Shprits and Ni*, 2009; *Orlova et al.*, 2012] that is formulated similarly to *Albert* [2005] and *Glauert and Horne* [2005]. The calculations include high-order resonances [*Ripoll and Mourenas*, 2012; *Mourenas and Ripoll*, 2012], and lifetimes were calculated using the method of *Albert and Shprits* [2009] that accounts for deep minimum of hiss scattering rates at intermediate pitch angles. Note that the latter is extrapolated below L = 3. The magnetic field model underlying the lifetime model is a dipole field for hiss since they are confined within the plasmasphere and the Tsyganenko 89 magnetic field model [*Tsyganenko*, 1989] for chorus waves as they act at higher Lshells.

The variation of hiss lifetimes with both energy and L shell are in agreement with previous works [e.g., *Meredith et al.*, 2007; *Mourenas and Ripoll*, 2012]. Similarly, electron lifetimes from chorus waves are taken from the recent work of *Orlova and Shprits* [2014], in which fits are also derived from full numerical simulations of $D_{\alpha\alpha}$. An extrapolation is made for $E > 2$ MeV. As statistics at high *Kp* was limited, the model may slightly underestimate the scattering rates for the times when *Kp* exceeds ~4 but gives rather accurate results for long-term calculations. The hiss model is activated within the plasmasphere while the chorus one is activated only outside the plasmasphere, with the plasmapause location being determined from *Carpenter and Anderson* [1992].

The radial diffusion model is also of two kinds: either we use the electrostatic diffusion coefficient D_{LLE} of the historical *Lyons and Thorne* [1973] that implicitly assumes $Kp = 1$ or the full model that is composed of both that D_{LLE} term, but corrected with the *Kp* dependence introduced in *Brautigam and Albert* [2000], combined with the electromagnetic diffusion coefficient D_{LLB} term of *Brautigam and Albert* [2000]. The latter model is the commonly used combination integrated in most 3-D radiation belt simulation, as in the VERB-3D code [*Shprits et al.*, 2009; *Subbotin et al.*, 2010] or in LANL DREAM3D [*Tu et al.*, 2013]. Nevertheless, a concern is that radial transport during individual events can exhibit large deviations from average transport rates because of nondiffusive character of the transport [e.g., *Ukhorskiy and Sitnov*, 2012; *Ukhorskiy et al.*, 2014] as well as substantial deviations due to impulsive transport for energies between tens and hundreds of keV [e.g., *Turner et al.*, 2015]. It may then not be an appropriate model to describe accurately filling or emptying of the slot region in particular during active times. Another example is the impulsive injection mechanism associated with substorm activity that involves non-diffusive transport and energization of electrons by coherent interaction with waves, which is not described by quasi-linear diffusion [e.g., *Li et al.*, 1998; *Gabrielse et al.*, 2012].

In this paper, we use two combination models for equation (5): first, the so-called *Lyons and Thorne* [1973] model made of D_{LLE}, hiss, and coulomb collision from *Lyons and Thorne* [1973] and second, the full model D_{LLE} and D_{LLB} combined with hiss and chorus pitch angle scattering from the most recent lifetimes [*Orlova et al.*, 2014; *Orlova and Shprits*, 2014]. The latter is called "Full model" and evaluated for $Kp = 1$, 3, and 6. The "characteristic time" for each model's radial diffusion coefficient and lifetimes are plotted in the (L, *E*) plane in Figure 1. Thanks to the *Kp*-dependent models, we are able to present steady state solutions for different geomagnetic conditions, although the steady state solution can only be physically achieved if the time to reach equilibrium is shorter than the time scale of the changes in geomagnetic activity.

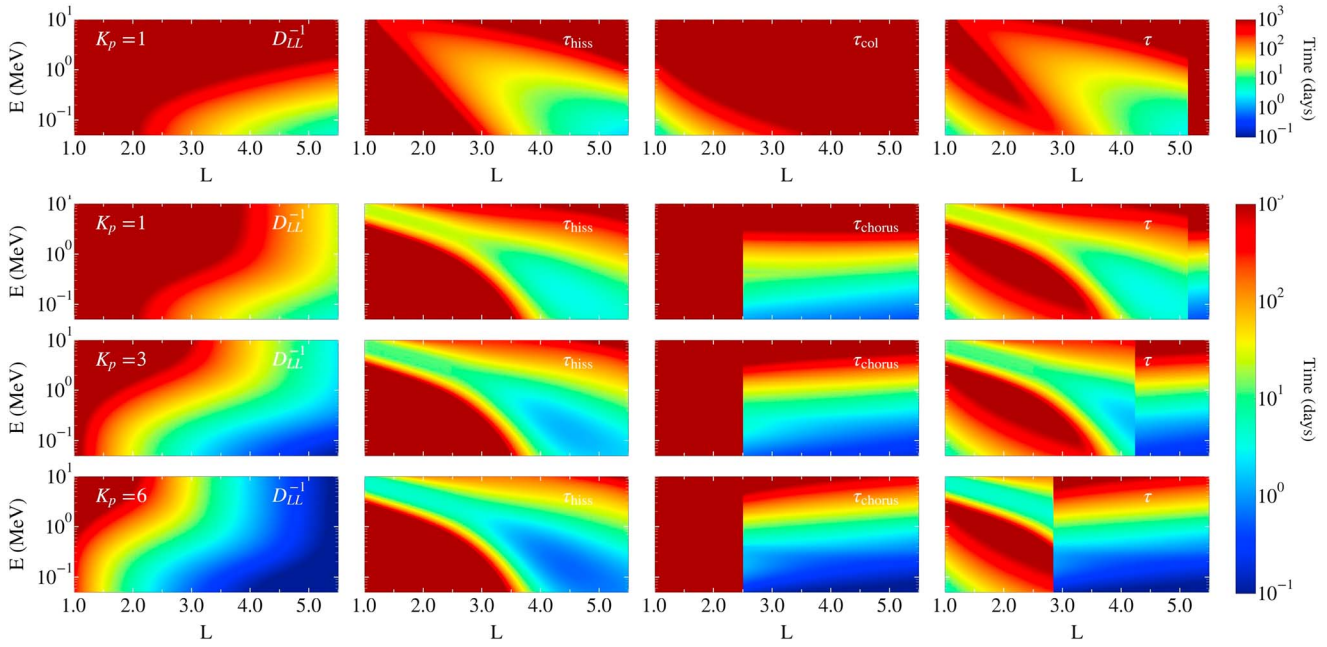

Figure 1. Radial diffusion rate, lifetimes due to hiss waves, lifetime due to Coulomb scattering, and harmonic sum of all three lifetimes in the (L shell, Energy) plane for $Kp = 1$, computed with the historical *Lyons and Thorne* [1973] model (first row) ($Kp = 1$). Radial diffusion rate, lifetimes due to hiss and chorus waves, and harmonic sum of all three lifetimes in the (L shell, energy) plane for (second row) $Kp = 1$, (third row) $Kp = 3$, and (fourth row) $Kp = 6$. Hiss is limited to inside the plasmasphere and chorus to outside, which creates a discontinuity at the plasmapause (right column). Hiss wave scattering will cause electron depletion along the diagonal $\log_{10}E \sim -L$.

At each *Kp* there is a plasmapause location, $L_{pp} = 5.6–0.46 * Kp$ [*Carpenter and Anderson*, 1992] that separates hiss and chorus activity and creates a discontinuity in the physical properties. The numerical scheme for discretizing equation (5) is based on a Crank-Nicholson scheme, which is second order in time and space. Equation (5) is classically solved for constant first and second invariants. The conversion of the PSD (defined from invariants) in flux $F = p^2 f$ (defined in pitch angle and energy), with p the electron's momentum, is done assuming a dipole field for simplicity, which allows to map any (μ, K) in (E, α) at a given L shell. More accurate computations could use the Tsyganenko 89 magnetic field model or the Tsyganenko 04 storm time model [*Tsyganenko and Sitnov*, 2005] at large *Kp* [e.g., *Tu et al*., 2014].

The boundary condition at L = 5.5 is the energy-dependent flux used in *Lyons and Thorne* [1973], which is given by $F(E) = AE^{-p}$ for $E < 0.05$ MeV and $F(E) = 1.163 \times 10^6 \exp(-E/0.2)$ for $E > 0.05$ MeV, where A is computed in order to preserve continuity at $E = 0.05$ MeV and F has units of #/(cm^2 s sr MeV).

Assuming no source at the inner boundary ($f(t, L_0) \sim 0$), the solution of equation (5) is a monotonic and decreasing PSD from a maximal value at the nonzero boundary condition at L_{max} because scattering imposes τ as always positive and $-f/\tau$ always negative. In other words, we have always $f(t, L_{max}) \geq f(t, L) \geq f(t, L_0)$. Therefore, in a dipole field, the flux increases with decreasing L shell as p^2, i.e., as L^{-3}, at most for a particle having a *ballistic* regime, defined here as fast particles entering the magnetosphere and conserving their distribution function $f(t, L) \sim f(t, L_{max}) = 1$ for all (t, L), i.e., $f(t, L)/f(t, L_{max}) \sim 1$.

We define the mean characteristic time as the harmonic average of all physical processes involved, $1/(\tau^{-1} + \tau_D{}^{-1})$, with $\tau = 1/(\tau_c{}^{-1} + \tau_H{}^{-1} + \tau_{Ch}{}^{-1})$ that includes all waves and Coulomb collisions (Figure S1) in the supporting information. Writing such a mean time consists of assuming all processes are decoupled, and the linear sum of each represents the global process, which is mathematically untrue but consistent with the approximations made to derive equation (5). This sum is always positive and represents the sum of the inverse of each of the smallest eigenvalues (slowest decaying modes) associated with the *i*th-diffusion matrix. At the plasmapause, hiss and chorus lifetimes are not continuous ($\tau_H(L_{pp}) \neq \tau_{Ch}(L_{pp})$), which create an abrupt discontinuity in the property (Figures 1 and S1 and S2). The ratio of both the characteristic time of radial diffusion (τ_D) and pitch angle (τ) is analogous to the Biot number (Jean-Baptiste Biot, 1780–1825) in transitional heat transfer. That number compares conduction, here, radial diffusion, with forced convection, here, the

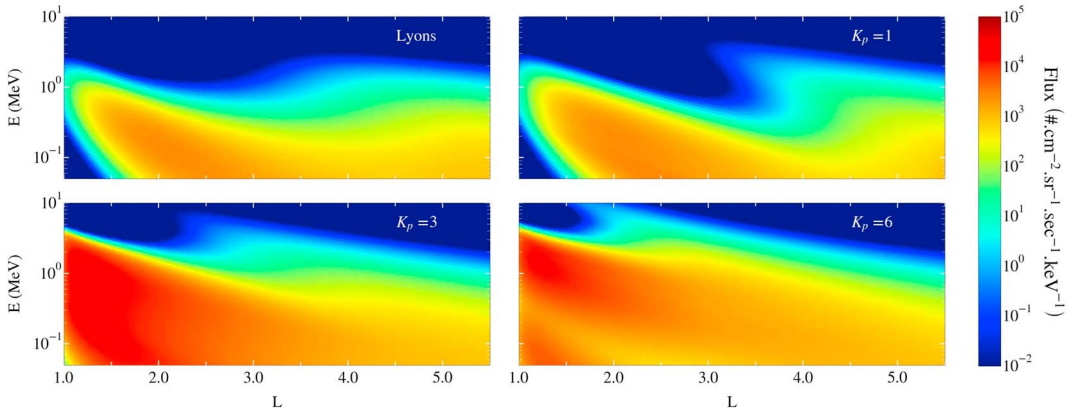

Figure 2. Equilibrium state of the electron flux in the (L shell, Energy) plane obtained with four models: (top left) the historical *Lyons and Thorne* [1973] model ($Kp = 1$) and (top right) the dynamic full model at $Kp = 1$, (bottom left) $Kp = 3$, and (bottom right) $Kp = 6$. The historical and full model equilibrium states are comparable at quiet times. The S structure of the full model at $Kp = 1$ is remarkable and similar to current observations from the Van Allen probes [*Reeves et al.*, 2016]. The slot shape is produced by the dependence of loss rate on energy and L shell.

f/τ loss term, with $1/\tau$ acting as a heat transfer exchange coefficient relaxing f to zero (Figure S2). These numbers are important when making the comparison with both the flux and the time to reach equilibrium.

3. Equilibrium Solutions

Equilibrium states are obtained by solving the steady form of equation (5) (with $\frac{\partial f}{\partial t} = 0$) by the simple resolution of the linear system formed by the diffusion operator and the source term, without any iteration. We use a mesh made of 200 μ values logarithmically sampled from $\mu = 10^{-5}$ to 10^{6}, and all results are presented at the second invariant $K = 0$. It gives an exact numerical solution, without a notion of time needed to reach that state. Equilibrium states are plotted in Figure 2 after projection from the (μ, K) plane into the (L, E) plane since it illustrates the energy dependence of both the slot and the location of the belts [*Lyons and Thorne*, 1973]. Readers should carefully consider low energies (e.g., $\mu \sim <100$ MeV/G at $Kp < 3$), since in our formulation we neglect the potentially dominant convective terms [*Thorne et al.*, 2007; *Shprits et al.*, 2015]. Figure 2 is complemented with 1-D line cuts plotted in Figure S3 for the four models following the (vintage) form of *Lyons and Thorne* [1973], either for different μ (on the left) or for different energies (on the right). The equilibrium structure of *Lyons and Thorne* [1973] is reproduced here. Providing equilibrium states in the (L, E) plane as Figure 2 is very useful to compare with recent observations. In particular, we notice an interesting S-shape form of the inner edge of the outer belt found for the equilibrium state at $Kp = 1$ (using the full model). A similar structure has been observed from the Van Allen Probes [*Reeves et al.*, 2016] and associated with the combination of radial diffusion and scattering from hiss waves [*Ripoll et al.*, 2016]. We prove here that indeed an S-shape structure can be formed at moderately low Kp for energies between 300 keV and 2 MeV, in the same range of energy as observed. The slot shape is strongly influenced by the dependence of electron loss rate on energy and L shell (unless radial transport is either too weak or too strong and hides the loss as discussed below). We see in the next section that the S shape is also seen during the dynamic evolution of the belts starting from a nonequilibrium initial state, and so it is not necessarily associated exclusively with an equilibrium state. The S shape is not obtained when using the original *Lyons and Thorne* [1973]. Since the hiss loss terms are quite similar in the original model and the full model, although lower in the original model (cf. Biot number's figure), we believe that the S shape is not produced by the original model due to the absence of D_{LLB}, which causes the radial transport at large L shells to be reduced, compared to the full model. We recall that D_{LLB} is considered a key aspect of the modeling of the outer belt dynamics [e.g., *Shprits et al.*, 2008; *Tu et al.*, 2013]. At higher Kp, the dynamics are controlled by fast radial transport that washes out the S shape at low energy (Figure 2, bottom line). Incoming electrons fill up the slot, but transport may be too strong, as suggested in *Kim et al.* [2011]. Only a slight plateau of high fluxes remains at L = 4, $E \sim 400$ keV, $Kp = 3$ and L = 3, $E \sim 1.5$ MeV at $Kp = 6$. As Kp increases, the S shape is reduced and shifted up to very high energy and lower L shells, remaining visible for $E > \sim 1.5$ MeV at $Kp = 3$ and $E > \sim 3$ MeV

at $Kp = 6$. It corresponds to L shell and energy at which radial transport gets slow enough so that losses from waves can dig their slot. One can check that the energy range of the slot matches well the L shells at which losses from hiss waves are strong, i.e., L~2 for 3–4 MeV electrons and L~3 for 1 MeV electrons [e.g., *Ripoll et al*., 2014a, 2014b, 2016]. We believe that the S shape is unlikely to be observed from moderate to active times because the energies at which an S shape is predicted become too high (>2 MeV for $Kp = 3$-6) and lacking in nature at the low L shell the structure is formed ($L < 2.5$ for $Kp = 3$-6) [*Fennell et al*., 2015]. The structure also shrinks to become very small at $Kp = 6$ (cf. the upper left corner of Figure 2, bottom line, right).

Finally, the inverse Biot number, the ratio of loss, and diffusion time scales (cf. Figure S2) give a rough idea of the shape of the fluxes. Fluxes are large for large inverse Biot numbers; i.e., diffusion is strong compared to scattering and reciprocally small for small inverse Biot numbers; i.e., scattering decays the fluxes.

4. Time to Reach the Equilibrium Value for Dynamic Solutions

Advancing in time (equation (5)) in order to obtain an equilibrium state is technically possible. According to the convergence residue chosen (often based on L_2 or L_∞ norms computed on the whole spatial domain), it can take tens to hundreds of physical years to reach convergence to the steady state. This is due to regions requiring very large time scales, associated with slow dynamics, for which reaching the equilibrium modulo a tiny residue is almost impossible. As an example, we found that it takes 10, 31, 76, 159, 865, and 229 years to reach convergence at $\mu = 3$, 10, 30, 50, 300, and 3000 MeV/G, respectively, at a residue of 10^{-8} using a restrictive double norm on the PSD.

Changing the residue or the norm definition changes the convergence time. The residue generally increases with μ (or E) except when there are slower wave process, as we see at $\mu = 300$ MeV/G. We now introduce a "local norm" that is simply the absolute value of the relative difference between the time-evolving PSD and the value of the equilibrium state, f^*, computed at each (L, μ) as a function of time. We define the time required to reach the value of the steady state solution, τ_{eq}, as the first time for which $|f(t, L, \mu) - f^*(L, \mu)|/|f^*(L, \mu)| < 0.1$, limited to 365 days.

The time that it takes for the PSD to first arrive within 10% of the value of the equilibrium state shall be referred to as "time to equilibrium." Parameter τ_{eq} is always defined because f^* is never zero due to nonzero boundary conditions at L = 5.5. For (L,E) locations at which nothing evolves and the PSD remains below 10^{-20}, τ_{eq} is not plotted and the figures show empty white regions. When the convergence criteria are satisfied, we choose plotting $f^*(\alpha, E)$ instead $f(t, \alpha, E)$. We present the dynamics and the time to reach equilibrium for two cases of interest in the next paragraphs.

4.1. Injection Following a Massive Dropout

We solve for the dynamics of an injection of electrons within an empty magnetosphere, as if a massive dropout had occurred previously. An example of a massive dropout is reported during the 17 March 2013 storm event [*Ukhorskiy et al*., 2014]. Results are presented in the (L, E) plane using the full model for three Kp indexes in Figure 3. The injection is driven by simultaneous radial diffusion and modulated by wave scattering, since either the radial diffusion is slow enough to let scattering occur at a scale of a few days (low Kp) or waves are strong when radial transport is fast (large Kp). (For comparison, readers can find a plot of the solution obtained with radial diffusion only in Figure S4.) At $Kp = 1$ (Figure 3, left column), the S-shape structure starts forming after 10 days, becoming well marked at 50 days (not shown), which proves, first, that this shape does not necessarily reflect an equilibrium state, and second, that it is caused by both scattering and transport. Hiss scattering causes the main (E, L) shape of the slot (see also *Ripoll et al*. [2016]). With radial diffusion only, that feature is not present (Figure S4). As time evolves, that structure becomes an increasingly obvious feature, as observed from the Van Allen Probes during quiet storm recovery periods [*Reeves et al*., 2016]. The steady state (or >100 day) solution is highly wave-dependent with a wide slot region and an outer belt made of mostly <500 keV electrons. The inner belt is not filled up before 100 days; however, a significant population of >800 keV electrons (up to 2 MeV) do eventually get into the inner belt, contrary to what is currently observed [*Fennell et al*., 2015], indicating that either radial diffusion is too strong or losses are too weak for these electrons. With the models in use, no *barrier* is observed for ultrarelativistic energies [*Baker et al*., 2014], and nothing stops the slow inward motion of the electrons below L = 2.8. The observed sharp gradient may be due to vanishing radial diffusion at lower L shells, stronger hiss losses in the slot region, or both

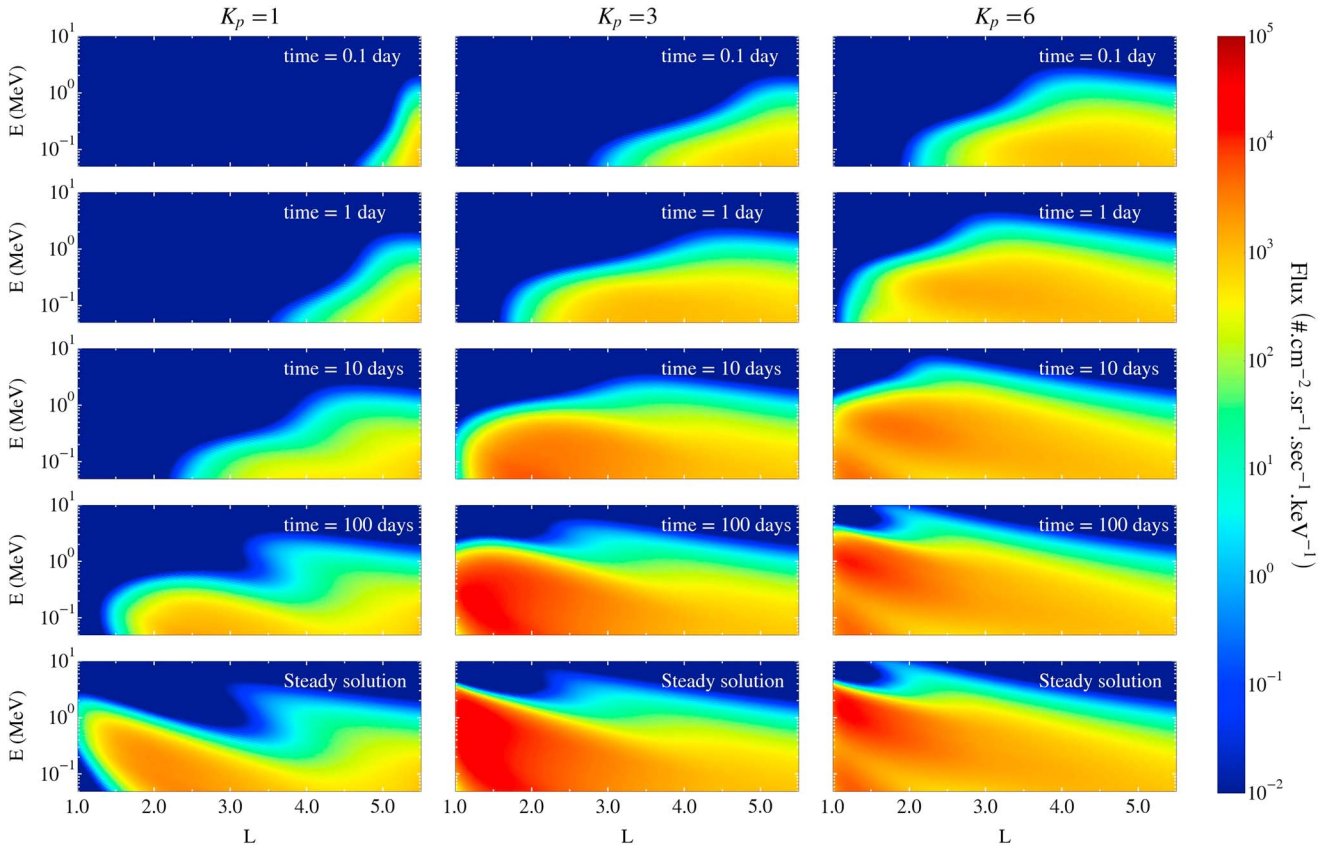

Figure 3. The dynamics of an injection into an empty belt is shown as the flux evolution in the (L shell, energy) plane for (left column) $Kp = 1$, (middle column) $Kp = 3$, and (right column) $Kp = 6$. For the low-energy electrons having $\tau \sim \infty$ and driven by fast radial transport, the transport is *ballistic* (i.e $f = f_{\mathrm{Lmax}} \sim 1$) and fluxes increase with L^{-3}. At quiet times, the S structure is an indicator of the competition between radial transport and losses. It is formed before the equilibrium state is reached. At $Kp = 1$, the formation of the slot by hiss scattering is well visible along the line $\log_{10}E = -1/2\,L + 3/2$. Figure S3 shows the same panels computed with radial diffusion only. The comparison attests of the effects of wave scattering at all *Kp*. At large *Kp* and with our models, nothing stops the inward motion of the ultra-relativistic electrons below L = 2.8. The values of the equilibrium state are generally reached after days of transport and losses (cf. next figure).

processes in an equilibrium state (or not in an equilibrium state). In our simulations, MeV electron flux is much lower at $Kp = 1$ than at higher *Kp*, in which case MeV electrons succeed in crossing the region of high scattering rates (due to D_{LLE}, which may be unrealistically high [*Kim et al.*, 2011]) and get trapped at lower L. At $Kp = 3$, fluxes would be homogeneously higher between L = 1.5 and 4.5 without wave scattering. The S shape is not visible for the first 100 days of simulation. A slot region in energy also appears for $Kp = 6$ for $L < 4$, immediately after 1 day, which would be interesting to look for in the data. The steady (or >100 day) solution at large *Kp* (>3) builds an inner belt that is constituted of >1 MeV electrons, which is not observed [*Fennell et al.*, 2015; *Baker et al.*, 2014]. The simulation result may be due to an assumption that active conditions persist longer than they would in reality, or to inaccuracies in the lifetime models at large *Kp* ($Kp > 5$), or to overestimation of the D_{LLE} at high *Kp* [*Kim et al.*, 2011].

We plot in Figure 4 the time, τ_{eq}, needed to reach the PSD value of the equilibrium state as a function of (L, *E*) to find out which electrons have reached an equilibrium value, and for which we infer that wave scattering balances radial diffusion. The comparison of the mean time (cf. Figure S1) with the equilibrium time, τ_{eq}, shows some similarities in the shape. Both have a characteristic complex *scissor* shape inside which low losses, small diffusion, and large trapping prevail. Inside these regions, hundreds of days (or more) are needed to reach the PSD value of the equilibrium state. On the other hand, the prescribed boundary condition at L = 5.5 implies that the PSD of the dynamic solution reaches the PSD value of the equilibrium state almost immediately. If the boundary was pushed further out to $L_{\mathrm{max}}^{\mathrm{new}}$, the equilibrium time would be increased by the time it takes for the electron dynamics to propagate from $L_{\mathrm{max}}^{\mathrm{new}}$ to L = 5.5. Increasing *Kp* shows that the faster the processes are, the less time is needed to reach the PSD value of the equilibrium state, which

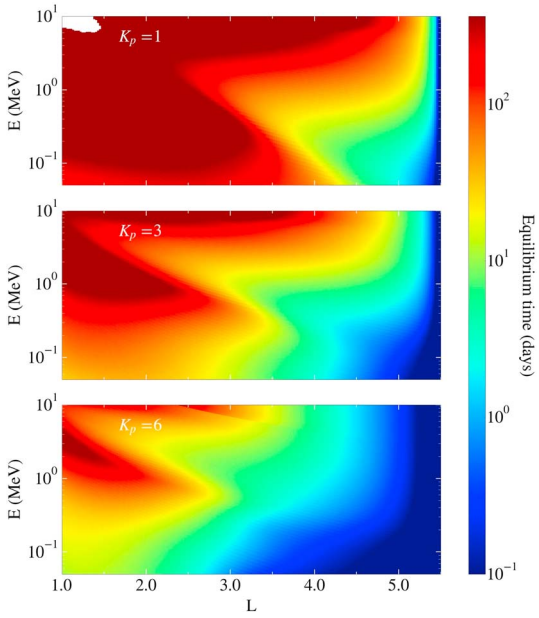

Figure 4. The time for injected electron at L = 5.5 to reach their equilibrium state plotted versus energy and L shell for (top) $Kp = 1$, (middle) $Kp = 3$, and (bottom) $Kp = 6$. The dark red regions correspond to times larger than 365 days, for which the computation has been stopped. It has a characteristic complex scissor shape inside which low losses, small diffusion, and large trapping prevail. Inside these regions, hundreds of days (or more) are needed to reach the PSD value of the equilibrium state. The equilibrium values may be reached only for selected L, *E*, and *Kp*. For instance, for $L < 4$, only small regions in (L, *E*) space can feasibly reach the value of the equilibrium state: $E \sim (200, 300)$ keV for L = (3.7, 4) at $Kp = 1$, $E =$ (0.6, 1) MeV for L = (3, 4) at $Kp = 3$, and $E \sim 300$ keV for L = (3.5, 4) at $Kp = 6$, assuming no new incoming electrons and stable geomagnetic conditions.

translates to smaller τ_{eq} for larger *Kp*. In general, obtaining the PSD values of the equilibrium state at all L, as assumed in *Lyons and Thorne* [1973], is very unlikely to occur with the models in use. The equilibrium values may be reached only for selected L, *E*, and *Kp*. For instance, regions in (L, *E*) space that can reach the values of the equilibrium state are due to hiss waves and form the slot along the line $\log_{10}E = -1/2\,L + 3/2$, matching the location of large loss rates (here, as well as in the next section).

In the next paragraphs, we assess from Figure 4 which electron population in the (L, *E*) plane could be at the equilibrium state according to the duration of stable magnetospheric conditions. For $Kp = 1$, the value of the equilibrium state could be reached in 1 to 10–20 days in the blue to green regions of Figure 4, corresponding to a prolonged geomagnetically quiet period, which may last for up to 10 days or longer. For such an extended quiet time, the source population is steady, and our simulations show that it is possible to reach equilibrium for *L* shells above approximately 4 and energies below ~600 keV. It corresponds to $E \sim 200$ keV starting as low as $L > 3.7$ for $Kp = 1$ or to $E < 400$ keV for $L > 4$. A last comment concerns the need to relate the time to reach the equilibrium state to the time required to reach MLT symmetrization, i.e., the time for an electron to drift around the Earth from a localized injection into a uniform thin shell. For quiet times ($Kp = 1$) in the slot (L = 3.1), *Liemohn et al.* [2012] have shown that it takes about 1 h for 1 MeV electrons and at least 6 h for ≤300 keV electrons to be uniformly organized in a thin shell, which is much lower than the times plotted here.

For $Kp = 3$, we assume that the value of the equilibrium state could be reached in 1 to 10–20 days in the blue to green regions. These elevated geomagnetic conditions may last for several days or even weeks, when solar wind activity is dominated by streams with high solar wind speed. In this case, equilibrium may be reached for $L > \sim 3$ for electrons with energies below ~600 keV. The dynamics of electrons at energies lower than approximately 100 keV during such disturbed conditions are most likely dominated by the convective transport (absent in the current modeling). For $L > 3.5$, the PSD value of the equilibrium state can be reached for $200 < E < 1$ MeV, with a quasi-static $Kp \sim 3$ lasting for 10 days. These regions are at equilibrium because both waves and diffusion are fast processes at this *Kp*.

During storm time conditions ($Kp = 6$), seen during coronal mass ejection driven storms, the elevated *Kp* lasts from a few hours to a day. The duration of such elevated *Kp* is limited to the time of passage of the magnetic cloud and to the period when magnetic field has a southward component. We choose then to look where τ_{eq} is on the order of 1 day or below (the blue region) to identify regions in (L, *E*) where the value of the equilibrium state can feasibly be reached. Our calculations show that the value of the equilibrium state may be reached only for $L > 4$ and $E > 300$ keV, provided that the boundary is kept constant. However, dropouts due to loss to the magnetopause, outward transport, and injections that can be significant at $L > 4$ would most likely not allow for the values of the equilibrium state to be reached, except for, possibly, a very narrow region in energy and L shell (i.e., ~400–500 keV at L = 4).

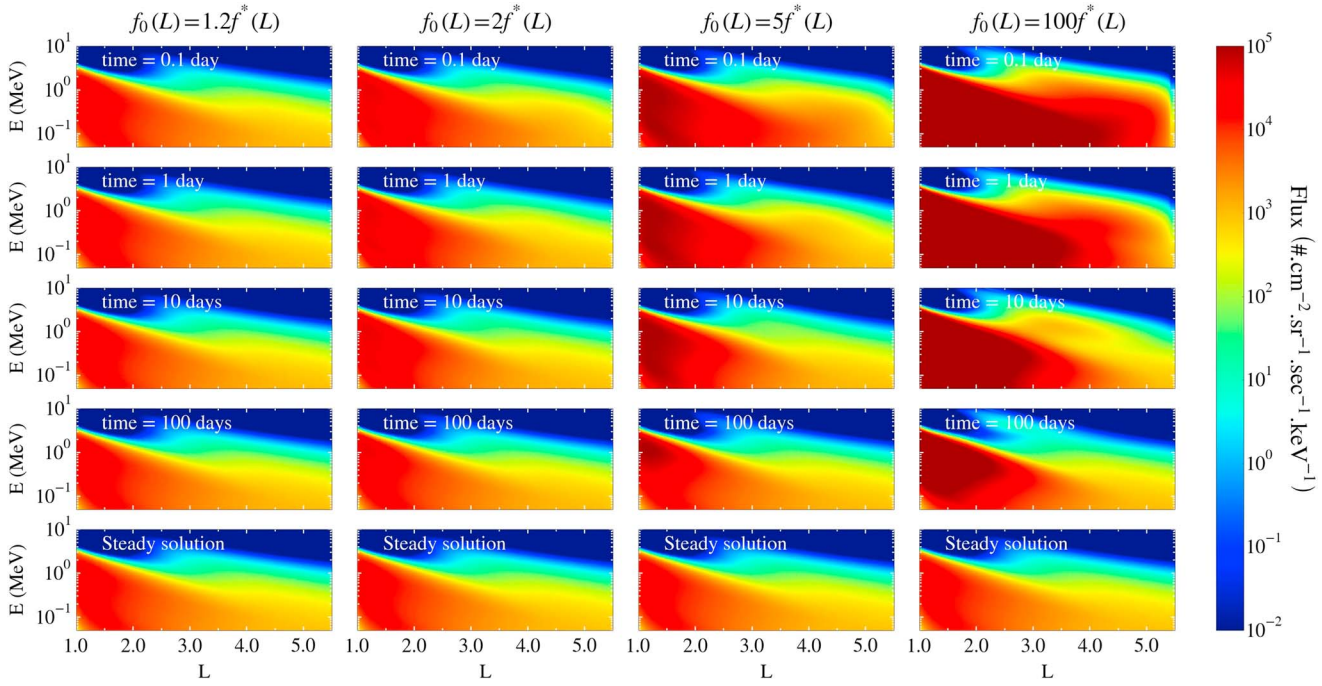

Figure 5. The dynamics of a saturated belt emptying until the equilibrium state is reached shown as the flux evolution in the (L shell, energy) plane for $Kp = 3$ (middle). Four different levels of initial conditions, assuming an equilibrium state f^* multiplied by 1.2, 2, 5, and 100, are used. Where processes are fast and close to the boundary conditions, the equilibrium state can be reached quickly. Otherwise, the saturated inner belt and inner slot regions ($L < 4$) are slowly evolving, with the time to reach the value of the equilibrium state plotted in the next figure.

Assuming that L shells larger than 4 are often perturbed by daily injections, as one can witness looking at long time periods (for instance, HEO observations over many years at L = 4 [e.g., *Ripoll et al.*, 2014b]), we now restrict our interest to the regions below L = 4. Only small regions in (L, *E*) space can feasibly reach the value of the equilibrium state: $E \sim (200, 300)$ keV for L = (3.7, 4) at $Kp = 1$, $E = (0.6, 1)$ MeV for L = (3, 4) at $Kp = 3$, and $E \sim 300$ keV for L = (3.5, 4) at $Kp = 6$, assuming no new incoming electrons.

4.2. Decaying Saturated Belts

Finally, we look at the dynamic evolution of a saturated magnetosphere, following a massive injection, losing its electrons from wave scattering and outward radial diffusion. The dynamics are shown for $Kp = 3$ in Figure 5 for four different levels of initial conditions, assuming an equilibrium state multiplied by 1.2, 2, 5, and 100. The time to decay to within 10% of the value of the unmodified equilibrium state is plotted in Figure 6 for $Kp = 1$, 3, and 6.

In general, the saturated inner belt and inner slot regions take hundreds of days and more before reaching the value of the equilibrium state. At $Kp = 1$, the equilibrium time below L = 3.5 is greater than hundreds of days, even with an initial state that is only 1.2 times the equilibrium state (first column of Figure 6). Reaching the value of the equilibrium state from this initial state becomes possible for $E \sim < 400$ keV and $L > 3.5$. As in the previous section, it is considered feasible to reach the value of the equilibrium state if τ_{eq} is less than 10 days (resp. 1 day) for $Kp = 3$ (resp. $Kp = 6$). This occurs for a large domain (all energies between L = 2 and L = 4) when the initial state is only a slight modification of the equilibrium state (first column of Figure 6).

When the initial state is twice the equilibrium state, it takes (almost) the same time to return to the value of the equilibrium state as it does when the initial state is an empty magnetosphere, i.e., the time to reach the values of the equilibrium state in Figure 6 (second column) is (almost) the same as Figure 4 (middle). It would be exactly the same if the boundary condition at L = 1 was not $f = 0$, since the boundary condition at L = 1 creates small losses that slightly change the solution at low L shells. The time to reach the value of the equilibrium state would not be the same for the 2× saturated and empty initial states if we had stronger Coulomb collisions at low L shells. Since the 2× saturated and empty initial states are quite similar, the conclusions for the empty initial state concerning the dynamics and the time to equilibrium apply to the 2× saturated case as well.

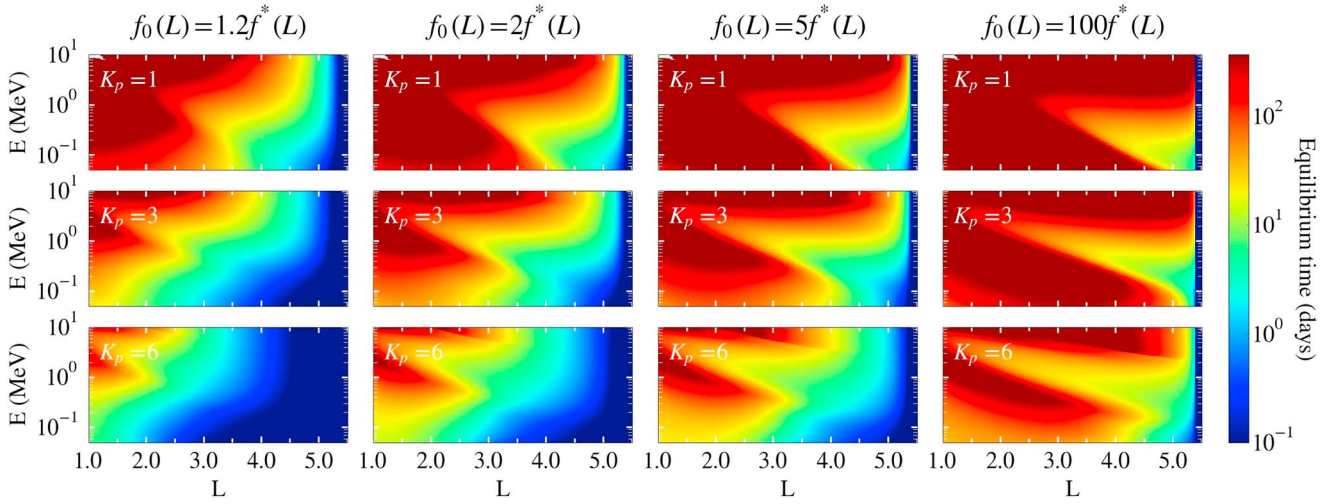

Figure 6. The time to reach the value of the equilibrium state starting from an initial state that is equal to the equilibrium state times a multiplicative constant (1.2 for column 1, 2 for column 2, 5 for column 3, and 100 for column 4), plotted versus energy and L shell for (top row) $Kp = 1$, (middle row) $Kp = 3$, (bottom row) $Kp = 6$. Reaching the value of the equilibrium state occurs for a large domain (all energies between L = 2 and L = 4) when the initial state is only a slight modification of the equilibrium state (first column). When the initial state is twice the equilibrium state (second left column), the time to reach the values of the equilibrium state is (almost) the same as Figure 4 (middle) (cf. explanation in the text). With a saturated magnetosphere (by a factor 5 or more), there are small windows of (L, *E*) in which it is feasible to reach the values of the equilibrium state below L = 4. The equilibrium state may be reached in regions where time scales between radial diffusion and pitch angle diffusion are comparable and are much shorter than the time scales of changes in magnetospheric conditions.

Otherwise, with a saturated magnetosphere (by a factor 5 or more), there are small windows of (L, *E*) in which it is feasible to reach the values of the equilibrium state below L = 4: a triangular region at $Kp = 3$ along the line of dominant hiss scattering ($\log_{10}E = -1/2\,L + 3/2$) for L = (3.5, 4) that includes *E* close to 1 MeV at $L = 3.5$ and *E* close to 400–500 keV at L = 4 and at $Kp = 6$, $E < 150$ keV for L = (3.5, 4). As shown previously, there is a chance

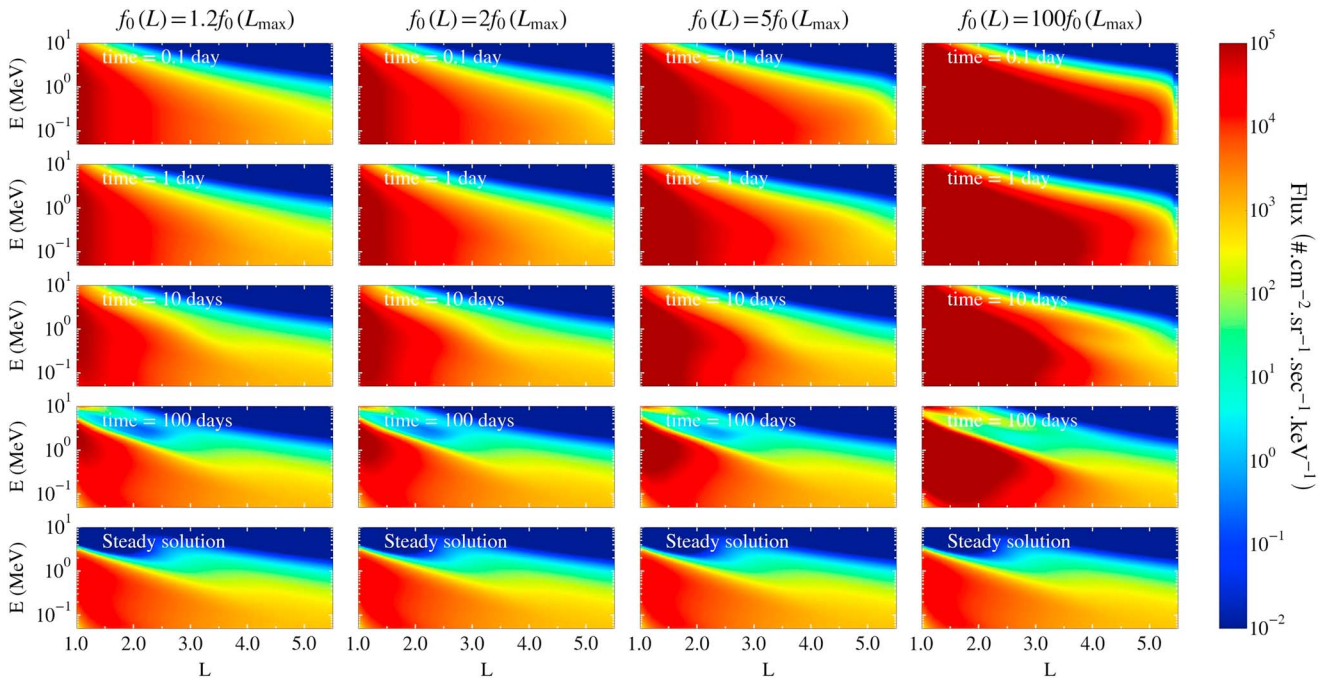

Figure 7. The dynamics of an uniformly saturated magnetosphere (with 1.2, 2, 5, and 100 times the values at L = 5.5, i.e., $f(t = 0,L) = \alpha f(L_{max})$) emptying until equilibrium is reached, shown as the flux evolution in the (L shell, energy) plane for $Kp = 3$. Solutions evolve similarly to Figure 5, with different shapes of the flux determined by the initial conditions. Outward radial diffusion is very efficient at removing excess electrons, with fast dynamics in the proximity of the boundary condition. Fast hiss scattering is visible along the main diagonal ($\text{Log}_{10}E \sim -L$) after 10 days.

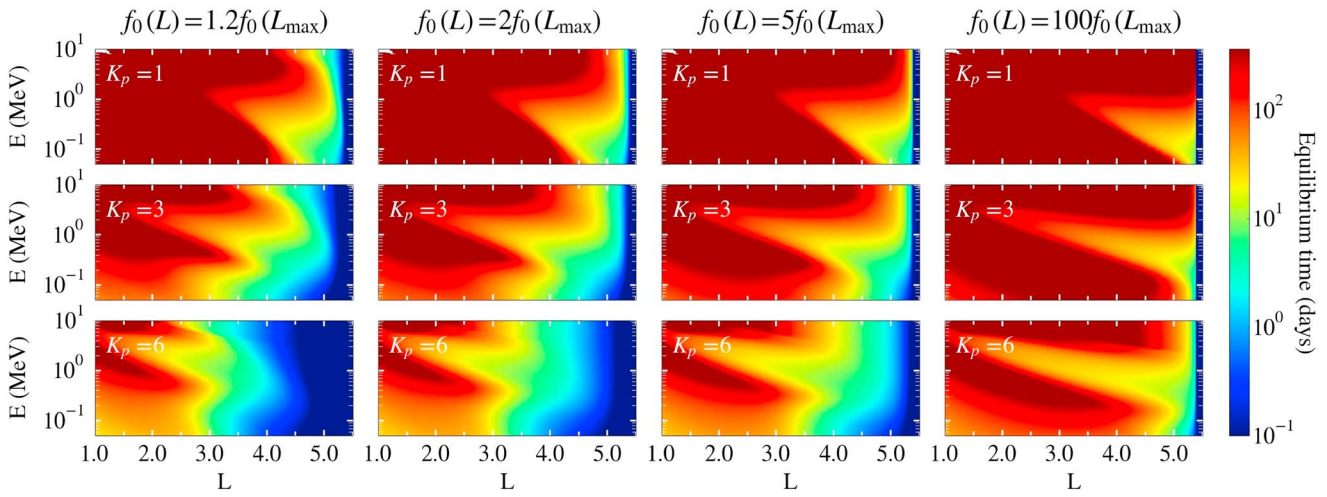

Figure 8. The time for a saturated belt to empty until reaching the equilibrium state, up to a year, plotted versus energy and L shell for (top row) $Kp = 1$, (middle row) $Kp = 3$, (bottom row) $Kp = 6$. The time to reach the value of the equilibrium state conserves its scissor shape with a necessary condition being fast hiss scattering. For a 2 orders of magnitude increase, the time to reach equilibrium is longer than characteristic times of relatively constant geomagnetic conditions. The assumption of steady state is then likely to be invalid at all L shells and energies.

to reach the value of the equilibrium state in regions where time scales between radial diffusion and pitch angle diffusion are comparable and are much shorter than the time scales of changes in magnetospheric conditions. Where processes are fast, the mean characteristic time (Figure 1) is small, and the time to equilibrium is the lowest. At large L shell ($L > 5$), outward radial diffusion is very efficient at removing excess electrons, and times to equilibrium are quite small due to the proximity of the boundary condition. We also looked at uniformly saturated magnetospheres, $f_0(L) = \alpha f(L_{max})$ for all L ($\alpha = 1.2$, 2, 5, and 100). The dynamics and time to equilibrium are plotted in Figures 7 and 8. Solutions evolve similarly, with different shapes of the flux determined by the initial conditions. The time to reach the value of the equilibrium state is longer because the dependence of the initial condition on L is less similar to the equilibrium state. However, its profile conserves its scissor shape with a necessary condition being fast hiss scattering.

Simulations of the evolution after fast massive injection ($f_0(L) = 100f(L_{max})$ and $f_0(L) = 100f^*$) clearly show that the time to reach equilibrium strongly depends on the initial condition. For typical increases by 2 orders of magnitude, our calculations show that the time to reach equilibrium is longer than characteristic times of relatively constant geomagnetic conditions. The assumption of steady state is then likely to be invalid at all L shells and energies. Finally, if one increases the flux boundary condition at L_{max} by a constant factor, then all fluxes are increased by that factor, but the time scales of the dynamics remain unchanged. Therefore, the time to reach equilibrium is not very sensitive to the boundary condition value itself, although it remains sensitive to the position of the boundary.

As a last sensitivity test, we modified the criteria on the local norm so that the value of the PSD only had to come within 50% of the value of the equilibrium state, rather than 10% as before. This test is performed to understand whether our 10% criterion could be too restrictive and lead to an overestimation of the times to reach the equilibrium state. Results are presented for $Kp = 3$ in Figure S5. We find that the time to reach the value of the equilibrium state conserves its characteristic *scissor* shape. It is slightly reduced as expected, with the 10 days region being shifted inward by 0.5 L shell or so. Regions where it is feasible to reach the value of the equilibrium state remain quite similar. However, intermediate states, at which $f^*(\alpha, E)$ replaces $f(t, \alpha, E)$ in the plots since the convergence criteria is satisfied, are found to be notably different from the previous ones, with denser regions being overestimated (resp. underestimated) when the initial condition is larger (resp. lower) than the steady state. This indicates that variations are still significant and that equilibrium is simply not reached yet.

5. Summary

In this paper, we model trapped electrons in the inner and outer radiation belts with a 1-D radial diffusion equation and lifetimes from Coulomb collisions, hiss, and chorus. The radial diffusion, hiss, and chorus

processes are all *Kp* and energy-dependent. We compute the equilibrium state, i.e., the PSD as a function of L shell, L, and energy, *E*, (or first invariant, μ), under the assumption of steady *Kp* for this model and contrast the equilibrium states with that computed by *Lyons and Thorne* [1973]. Next, starting from initial states of the PSD that simulate a recently depleted or saturated inner magnetosphere, we compute the time-dependent PSD using inner and outer boundary conditions and, for each (L, *E*), calculate the time that it takes for the PSD to first come within 10% of the value of the equilibrium state, which we call the time to equilibrium. If the time to equilibrium for a given (L, *E*) is less than the amount of time reasonable to suppose that a steady value of *Kp* could be observed, we propose that it is feasible to reach the equilibrium value at that particular (L, *E*), and we present regions in (L, *E*) at different *Kp* where this occurs. The analysis allows us to determine when the steady state assumption can be used to simplify the calculation of the state of the radiation belts, for instance, in space weather computations. When the time-dependent PSD is plotted in the (L, *E*) plane at a given time at moderately low *Kp*, a characteristic S shape near the inner edge of the outer belt appears that is similar to recent observations from the Van Allen Probes [*Reeves et al*., 2016; *Ripoll et al*., 2016]. This shape is also seen in the equilibrium state. It is due to the combination of radial transport and loss, with a structure in the (L, *E*) plane dictated by the electron loss rate dependence in both energy and L shell. Equilibrium electron flux profiles follow the Biot number, with large Biot number corresponding to low fluxes and low Biot number to large fluxes. The time to reach equilibrium is a complex quantity that is governed by the initial state of the belts, the property of the dynamics (diffusion coefficients), and the size of the domain of computation. It has to be compared to the time scale of the changes of the magnetospheric conditions. Its structure shows a rather complex *scissor* form in the (L, *E*) plane, with trapping regions in the inner belt and at high energy, where the dynamics are slower. It is shown that it is only feasible to reach the value of the equilibrium state for selected locations in energy, radial distance, and geomagnetic activity space. While the periods when *Kp* stays relatively constant may be longer at very quiet geomagnetic conditions, the time to reach equilibrium is shown to be shorter during disturbed geomagnetic conditions ($Kp \geq 3$) when diffusion rates are higher. The time to reach equilibrium also tends to be shorter at higher L shells, where radial diffusion is faster and also at energies where waves provide most of the scattering. Equilibrium regions due to hiss waves and forming the slot are along the line $\log_{10}E = -1/2\,\mathrm{L} + 3/2$. Where processes are fast, the mean characteristic time is small and the time to reach equilibrium is the lowest. However, at high L shells, variations in the population due to transport and loss to the magnetopause may not allow for reaching the value of the equilibrium state. For $Kp = 1$, as during extended solar minimum periods, our simulations show that it is possible to reach the value of the equilibrium state for L shells above approximately 4 and energies below ~600 keV. For stable $Kp = 3$, as during high solar wind streams, the value of the equilibrium state may be reached for $200\,\mathrm{keV} < E < 1\,\mathrm{MeV}$ for $\mathrm{L} > 3.5$. During storm time conditions, our calculations show that the value of the equilibrium state may be reached only for $\mathrm{L} > 4$ and $E > 300\,\mathrm{keV}$ but, either magnetopause losses, outward transport, and/or injections would most likely not allow for the value of the equilibrium state to be reached, except for, possibly, a very narrow region in energy and L shell. Restricting our interest to the deepest regions below $\mathrm{L} = 4$, which are less disturbed by the outer belt dynamics, only small regions in (L, *E*) space can reach the value of the equilibrium state: $E \sim (200, 300)$ keV for $\mathrm{L} = [3.7, 4]$ at $Kp = 1$, $E \sim (0.6, 1)$ MeV for $\mathrm{L} = (3, 4)$ at $Kp = 3$, and $E \sim 300$ keV for $\mathrm{L} = (3.5, 4)$ at $Kp = 6$, assuming no new incoming electrons. At low or moderate *Kp*, we believe that it may be observable in nature for these energies after ~10 days of stable conditions. Simulations of the evolution after fast massive injections show that the time to reach the value of the equilibrium state is longer than times of relatively constant geomagnetic conditions, and thus, the assumption of steady state is then unlikely to be valid for entire belts at all radial distances and energies (L, *E*).

Acknowledgments

This work was performed under the auspices of an agreement between CEA/DAM and NNSA/DP on cooperation on fundamental science. G.S.C. would like to acknowledge the Los Alamos National Laboratory LDRD program. Y.Y.S. would like to acknowledge support by the NASA grants NNX10AK99G and NNX13AE34G, NSF grant 443869-YS-21686, UC Lab Fee grant 116720, and Horizon 2020 637302. For further information or right to access to the material used in this paper, readers can contact the authors.

References

Albert, J. M. (2005), Evaluations of quasi-linear diffusion coefficients for whistler mode waves in a plasma with arbitrary density ratio, *J. Geophys. Res.*, *110*, A03218, doi:10.1029/2004JA010844.

Albert, J. M., and Y. Y. Shprits (2009), Estimates of lifetimes against pitch angle diffusion, *J. Atmos. Sol. Terr. Phys.*, *71*, 1647–1652, doi:10.1016/j.jastp.2008.07.004.

Albert, J. M., N. P. Meredith, and R. B. Horne (2009), Three-dimensional diffusion simulation of outer radiation belt electrons during the 9 October 1990 magnetic storm, *J. Geophys. Res.*, *114*, A09214, doi:10.1029/2009JA014336.

Baker, D. N., S. G. Kanekal, R. B. Horne, N. P. Meredith, and S. A. Glauert (2007), Low-altitude measurements of 2–6 MeV electron trapping lifetimes at $1.5 \leq \mathrm{L} \leq 2.5$, *Geophys. Res. Lett.*, *34*, L20110, doi:10.1029/2007GL031007.

Baker, D. N., et al. (2013), A long-lived relativistic electron storage ring embedded in Earth's outer Van Allen belt, *Science*, *340*, 186–190, doi:10.1126/science.1233518.

Baker, D. N., et al. (2014), An impenetrable barrier to ultrarelativistic electrons in the Van Allen radiation belts, *Nature*, *515*, 531–534, doi:10.1038/nature13956.

Brautigam, D. H., and J. M. Albert (2000), Radial diffusion analysis of outer radiation belt electrons during the 9 October 1990 magnetic storm, *J. Geophys. Res.*, *105*, 291–309, doi:10.1029/1999JA900344.

Carpenter, D. L., and R. R. Anderson (1992), An ISEE/whistler model of equatorial electron density in the magnetosphere, *J. Geophys. Res.*, *97*, 1097–1108, doi:10.1029/91JA01548.

Fennell, J. F., S. Kanekal, and J. L. Roeder (2012), Storm responses of radiation belts during solar cycle 23: HEO satellite observations, in *Dynamics of the Earth's Radiation Belts and Inner Magnetosphere*, *Geophys. Monogr. Ser.*, vol. 199, edited by D. Summers et al., pp. 371–384, AGU, Washington, D. C.

Fennell, J. F., S. G. Claudepierre, J. B. Blake, T. P. O'Brien, J. H. Clemmons, D. N. Baker, H. E. Spence, and G. D. Reeves (2015), Van Allen Probes show that the inner radiation zone contains no MeV electrons: ECT/MagEIS data, *Geophys. Res. Lett.*, *42*, 1283–1289, doi:10.1002/2014GL062874.

Friedel, R. H. W., A. Korth, and G. Kremser (1996), Substorm onsets observed by CRRES: Determination of energetic particle source regions, *J. Geophys. Res.*, *101*(A6), 13,137–13,154, doi:10.1029/96JA00399.

Gabrielse, C., V. Angelopoulos, A. Runov, and D. L. Turner (2012), The effects of transient, localized electric fields on equatorial electron acceleration and transport toward the inner magnetosphere, *J. Geophys. Res.*, *117*, A10213, doi:10.1029/2012JA017873.

Glauert, S. A., and R. B. Horne (2005), Calculation of pitch angle and energy diffusion coefficients with the PADIE code, *J. Geophys. Res.*, *110*, A04206, doi:10.1029/2004JA010851.

Kim, K.-C., Y. Shprits, D. Subbotin, and B. Ni (2011), Understanding the dynamic evolution of the relativistic electron slot region including radial and pitch angle diffusion, *J. Geophys. Res.*, *116*, A10214, doi:10.1029/2011JA016684.

Korth, A., R. H. W. Friedel, C. G. Mouikis, J. F. Fennell, J. R. Wygant, and H. Korth (2000), Comprehensive particle and field observations of magnetic storms at different local times from the CRRES spacecraft, *J. Geophys. Res.*, *105*, 18, 729–18,740, doi:10.1029/1999JA000430.

Li, X., D. N. Baker, M. Temerin, D. Reeves, and R. D. Belian (1998), Simulation of dispersionless injections and drift echoes of energetic electrons associated with substorms, *Geophys. Res. Lett.*, *25*(20), 3763–3766, doi:10.1029/1998GL900001.

Li, Z., M. Hudson, A. Jaynes, A. Boyd, D. Malaspina, S. Thaller, J. Wygant, and M. Henderson (2014), Modeling gradual diffusion changes in radiation belt electron phase space density for the March 2013 Van Allen Probes case study, *J. Geophys. Res. Space Physics*, *119*, 8396–8403, doi:10.1002/2014JA020359.

Liemohn, M. W., S. Xu, S. Yan, M.-C. Fok, and Q. Zheng (2012), Time scales for localized radiation belt injections to become a thin shell, in *Dynamics of the Earth's Radiation Belts and Inner Magnetosphere*, *Geophys. Monogr. Ser.*, vol. 199, pp. 161–175, AGU, Washington, D. C., doi:10.1029/2012GM001335.

Lyons, L. R., and R. M. Thorne (1973), Equilibrium structure of radiation belt electrons, *J. Geophys. Res.*, *78*(13), 2142–2149, doi:10.1029/JA078i013p02142.

Lyons, L. R., R. M. Thorne, and C. F. Kennel (1972), Pitch-angle diffusion of radiation belt electrons within the plasmasphere, *J. Geophys. Res.*, *77*(19), 3455–3474, doi:10.1029/JA077i019p03455.

Meredith, N. P., R. B. Horne, S. A. Glauert, R. M. Thorne, D. Summers, J. M. Albert, and R. R. Anderson (2006), Energetic outer zone electron loss timescales during low geomagnetic activity, *J. Geophys. Res.*, *111*, A05212, doi:10.1029/2005JA011516.

Meredith, N. P., R. B. Horne, S. A. Glauert, and R. R. Anderson (2007), Slot region electron loss timescales due to plasmaspheric hiss and lightning-generated whistlers, *J. Geophys. Res.*, *112*, A08214, doi:10.1029/2007JA012413.

Meredith, N. P., R. B. Horne, S. A. Glauert, D. N. Baker, S. G. Kanekal, and J. M. Albert (2009), Relativistic electron loss timescales in the slot region, *J. Geophys. Res.*, *114*, A03222, doi:10.1029/2008JA013889.

Mourenas, D., and J.-F. Ripoll (2012), Analytical estimates of quasi-linear diffusion coefficients and electron lifetimes in the inner radiation belt, *J. Geophys. Res.*, *117*, A01204, doi:10.1029/2011JA016985.

O'Brien, T. P., S. G. Claudepierre, J. B. Blake, J. F. Fennell, J. H. Clemmons, J. L. Roeder, H. E. Spence, G. D. Reeves, and D. N. Baker (2014), An empirically observed pitch-angle diffusion eigenmode in the Earth's electron belt near L* = 5.0, *Geophys. Res. Lett.*, *41*, 251–258, doi:10.1002/2013GL058713.

Orlova, K., and Y. Shprits (2014), Model of lifetimes of the outer radiation belt electrons in a realistic magnetic field using realistic chorus wave parameters, *J. Geophys. Res. Space Physics*, *119*, 770–780, doi:10.1002/2013JA019596.

Orlova, K., M. Spasojevic, and Y. Shprits (2014), Activity-dependent global model of electron loss inside the plasmasphere, *Geophys. Res. Lett.*, *41*, 3744–3751, doi:10.1002/2014GL060100.

Orlova, K. G., Y. Y. Shprits, and B. Ni (2012), Bounce-averaged diffusion coefficients due to resonant interaction of the outer radiation belt electrons with oblique chorus waves computed in a realistic magnetic field model, *J. Geophys. Res.*, *117*, A07209, doi:10.1029/2012JA017591.

Ozeke, L. G., I. R. Mann, K. R. Murphy, I. Jonathan Rae, and D. K. Milling (2014), Analytic expressions for ULF wave radiation belt radial diffusion coefficients, *J. Geophys. Res. Space Physics*, *119*, 1587–1605, doi:10.1002/2013JA019204.

Reeves, G. D., et al. (2016), Energy dependent dynamics of keV to MeV electrons in the inner zone, outer zone, and slot regions, *J. Geophys. Res. Space Physics*, *121*, 397–412, doi:10.1002/2015JA021569.

Ripoll, J.-F., and D. Mourenas (2012), High-energy electron diffusion by resonant interactions with whistler mode hiss, in *Dynamics of the Earth's Radiation Belts and Inner Magnetosphere*, *Geophys. Monogr. Ser.*, vol. 199, doi:10.1029/2012GM001309.

Ripoll, J.-F., J. M. Albert, and G. S. Cunningham (2014a), Electron lifetimes from narrowband wave-particle interactions within the plasmasphere, *J. Geophys. Res. Space Physics*, *119*, 8858–8880, doi:10.1002/2014JA020217.

Ripoll, J.-F., Y. Chen, J. F. Fennell, and R. H. W. Friedel (2014b), On long decays of electrons in the vicinity of the slot region observed by HEO3, *J. Geophys. Res. Space Physics*, *119*, 460–478, doi:10.1002/2014JA020449.

Ripoll, J.-F., et al. (2016), Reproducing the observed energy-dependent structure of Earth's electron radiation belts during storm recovery with an event-specific diffusion model, *Geophys. Res. Lett.*, *43*, 5616–5625, doi:10.1002/2016GL068869.

Roederer, J. G. (1970), *Dynamics of Geomagnetically Trapped Radiation*, Springer, New York.

Roederer, J. G., and H. Zhang (2014), *Dynamics of Magnetically Trapped Particles*, 2nd ed., Springer, New York, doi:10.1007/978-3-642-41530-2.

Selesnick, R. S. (2015), Measurement of inner radiation belt electrons with kinetic energy above 1 MeV, *J. Geophys. Res. Space Physics*, *120*, 8339–8349, doi:10.1002/2015JA021387.

Schulz, M., and L. Lanzerotti (1974), *Particle Diffusion in the Radiation Belts*, Springer, New York.

Shprits, Y. Y., and B. Ni (2009), Dependence of the quasi-linear scattering rates on the wave normal distribution of chorus waves, *J. Geophys. Res.*, *114*, A11205, doi:10.1029/2009JA014223.

Shprits, Y. Y., and R. M. Thorne (2004), Time dependent radial diffusion modeling of relativistic electrons with realistic loss rates, *Geophys. Res. Lett.*, *31*, L08805, doi:10.1029/2004GL019591.

Shprits, Y. Y., R. M. Thorne, G. D. Reeves, and R. Friedel (2005), Radial diffusion modeling with empirical lifetimes: Comparison with CRRES observations, *Ann. Geophys.*, *23*(4), 1467–1471, doi:10.5194/angeo-23-1467-2005.

Shprits, Y. Y., D. A. Subbotin, N. P. Meredith, and S. R. Elkington (2008), Review of modeling of losses and sources of relativistic electrons in the outer radiation belts: II. Local acceleration and loss, *J. Atmos. Sol. Terr. Phys.*, *70*(14), 1694–1713, doi:10.1016/j.jastp.2008.06.014.

Shprits, Y. Y., D. Subbotin, and B. Ni (2009), Evolution of electron fluxes in the outer radiation belt computed with the VERB code, *J. Geophys. Res.*, *114*, A11209, doi:10.1029/2008JA013784.

Shprits, Y. Y., D. Subbotin, A. Drozdov, M. E. Usanova, A. Kellerman, K. Orlova, D. N. Baker, D. L. Turner, and K.-C. Kim (2013), Unusual stable trapping of the ultra-relativistic electrons in the Van Allen radiation belts, *Nat. Phys.*, *9*, 699–703, doi:10.1038/nphys2760.

Shprits, Y. Y., A. C. Kellerman, A. Y. Drozdov, H. A. Spence, G. D. Reeves, and D. N. Baker (2015), Combined convective and diffusive simulations: VERB-4D comparison with March 17, 2013 Van Allen Probes Observations, *Geophys. Res. Lett.*, *42*, 9600–9608, doi:10.1002/2015GL065230.

Subbotin, D. A., Y. Y. Shprits, and B. Ni (2010), Three-dimensional VERB radiation belt simulations including mixed diffusion, *J. Geophys. Res.*, *115*, A03205, doi:10.1029/2009JA015070.

Thorne, R. M., Y. Y. Shprits, N. P. Meredith, R. B. Horne, W. Li, and L. R. Lyons (2007), Refilling of the slot region between the inner and outer electron radiation belts during geomagnetic storms, *J. Geophys. Res.*, *112*, A06203, doi:10.1029/2006JA012176.

Tsyganenko, N. A. (1989), A magnetospheric magnetic field model with a warped tail current sheet, *Planet. Space Sci.*, *37*, 5–20, doi:10.1016/0032-0633(89)90066-4.

Tsyganenko, N. A., and M. I. Sitnov (2005), Modeling the dynamics of the inner magnetosphere during strong geomagnetic storms, *J. Geophys. Res.*, *110*, A03208, doi:10.1029/2004JA010798.

Tu, W., X. Li, Y. Chen, G. D. Reeves, and M. Temerin (2009), Storm-dependent radiation belt electron dynamics, *J. Geophys. Res.*, *114*, A02217, doi:10.1029/2008JA013480.

Tu, W., G. S. Cunningham, Y. Chen, M. G. Henderson, E. Camporeale, and G. D. Reeves (2013), Modeling radiation belt electron dynamics during GEM challenge intervals with the DREAM3D diffusion model, *J. Geophys. Res. Space Physics*, *118*, 6197–6211, doi:10.1002/jgra.50560.

Tu, W., G. S. Cunningham, Y. Chen, S. K. Morley, G. D. Reeves, J. B. Blake, D. N. Baker, and H. Spence (2014), Event specific chorus wave and electron seed population models in DREAM3D using the Van Allen Probes, *Geophys. Res. Lett.*, *41*, 1359–1366, doi:10.1002/2013GL058819.

Turner, D. L., V. Angelopoulos, W. Li, M. D. Hartinger, M. Usanova, I. R. Mann, J. Bortnik, and Y. Shprits (2013), On the storm-time evolution of relativistic electron phase space density in Earth's outer radiation belt, *J. Geophys. Res. Space Physics*, *118*, 2196–2212, doi:10.1002/jgra.50151.

Turner, D. L., et al. (2015), Energetic electron injections deep into the inner magnetosphere associated with substorm activity, *Geophys. Res. Lett.*, *42*, 2079–2087, doi:10.1002/2015GL063225.

Ukhorskiy, A. Y., and M. I. Sitnov (2012), Dynamics of radiation belt particles, *Space Sci. Rev.*, 545–578, doi:10.1007/s11214-012-9938-5.

Ukhorskiy, A. Y., M. I. Sitnov, R. M. Millan, B. T. Kress, and D. C. Smith (2014), Enhanced radial transport and energization of radiation belt electrons due to drift orbit bifurcations, *J. Geophys. Res. Space Physics*, *119*, 163–170, doi:10.1002/2013JA019315.

Walt, M. (1970), Radial diffusion of trapped particles, in *Particles and Fields in the Magnetosphere*, edited by B. M. McCormac, pp. 410, D. Reidel, Dordrecht, Holland.